ACS OMEGA

http://pubs.acs.org/journal/acsodf

Article

Exploring the Cobalt–Histidine Complex for Wide-Ranging Colorimetric O_2 Detection

Abhishek Saini, Surabhi Rai, Debabrata Maiti,* and Arnab Dutta*

Cite This: *ACS Omega* 2022, 7, 27734–27741

Read Online

ACCESS | Metrics & More | Article Recommendations | Supporting Information

ABSTRACT: Developing a robust, cost-effective, and user-friendly sensor for monitoring molecular oxygen (O_2) ranging from a minute to a medically relevant level (85−100%) in a stream of flowing breathable gas is vital in various industrial domains. Here, we report an innovative application of the cobalt(L-histidine)$_2$ complex, a bioinspired model of O_2-carrying metalloproteins, for rapid and reliable sensing of O_2 from 0 to 100% saturation levels under realistic conditions. We have established two distinct colorimetric O_2 detection techniques, which can be executed with the use of a common smartphone camera and readily available color-detecting software. A series of spectroscopic experiments were performed to demonstrate the molecular-level alteration in cobalt(L-histidine)$_2$ following its exposure to oxygen, leading to an exclusive pink-to-brown color change. Therefore, this study establishes a template for designing bioinspired molecular complexes for O_2 sensing, leading to practical and straightforward solutions. This metal-amino acid complex's broad-spectrum sensing of O_2 has widened the scope of bioinspired model complexes for divergent applications in industrial sectors.

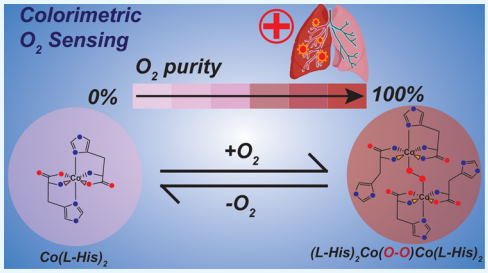

INTRODUCTION

Oxygen (O_2) gas is reckoned as one of the essential components for the survival of life on earth. The influence of molecular oxygen has stretched beyond biology and found widespread applications in the medicinal, metallurgical, and construction industries.[1,2] Hence, quantitative measurement of oxygen at variable levels remains a prime analytical interest. The detection of oxygen concentration in the lower range (0.1−10%) is important for food packaging as it helps in controlling the microbial and oxidative spoilage of the product.[3−6] The detection of a higher concentration of O_2 has emerged as a key factor for the medical life-support system that has certainly been realized during the recent COVID-19 pandemic scenario. Here, the presence of 92−96% optimal oxygen saturation (SpO_2) in supplemental oxygen is found to be critical for the recovery and well-being of COVID-19-infected patients.[7] Hence, accurate and user-friendly oxygen purity-detecting technologies have garnered more consideration now than ever. To date, several methodologies have been devised to sense O_2 via partial pressure, electrical, or photochemical signals. Nanoparticle-based materials are the popular choice for developing such technologies, owing to their potential use in the form of practically viable polymer matrices and films.[8a−d] However, these processes typically require expensive and delicate instruments to elude their potential mass consumption.[9] Recently, colorimetric sensing techniques have emerged as a popular O_2 diagnostic method that even includes commonly used smartphones and other mobile computing devices.[10] Evans and co-workers reported a luminescence-based colorimetric oxygen sensor mimicking a *traffic light* behavior. However, the rapid quenching of the deployed fluorophore restricted the specific differentiation of varying O_2 concentrations.[11] An assembly of cadmium telluride (CdTe) quantum dots (QDs) and [meso-tetrakis-(pentafluorophenyl)-porphyrinato] platinum (II) was also utilized for generating an optical sensor strip for O_2. This reversibly active strip efficiently identified molecular oxygen at diverse concentrations although its sensitivity failed beyond a 50% O_2 level.[12] All these oxygen sensors known so far are active in a certain range of oxygen levels and unable to detect oxygen in its all concentrations, thus limiting their use in several aspects. Thus, the search for fabricating a colorimetric oxygen sensor continues that can precisely quantify the amount of oxygen present in the system in a broad spectrum range from 0.1 to 100%. These types of sensors not only act as a boon in severe COVID 19 situations but can also be used for diversified purposes from health care to other industries.

Oxygen molecules are transported in biology via discrete O_2-carrier metalloproteins, such as hemoglobin, hemerythrin, and hemocyanin.[13−15] All these proteins exist in two distinct forms: O_2-bound oxy and O_2-less deoxy. Interestingly, these two forms exhibit distinctively separate colors, which can be reckoned as a template for colorimetric O_2 sensing. The direct usage of the natural metalloproteins for O_2 detection is

Received: June 22, 2022
Accepted: July 21, 2022
Published: July 29, 2022

Scheme 1. Formation of Deoxy-M and its conversion to the Oxy-M following its interaction with the molecular oxygen

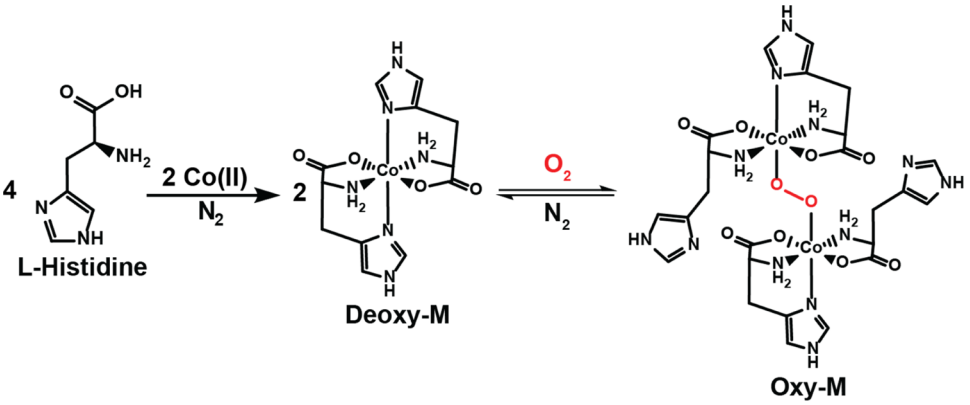

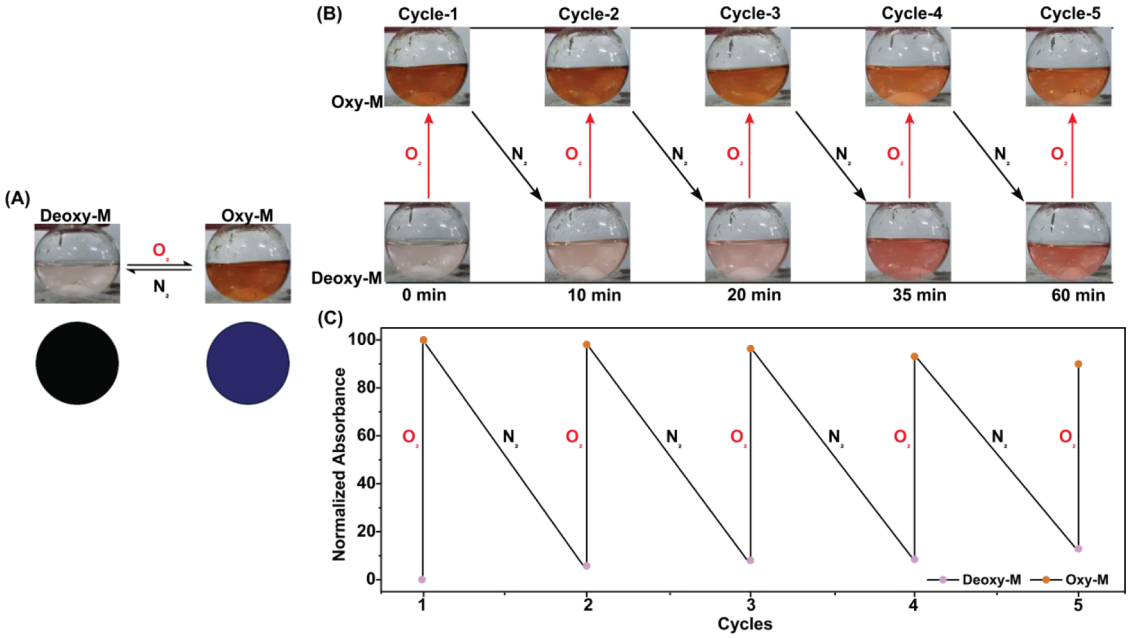

Figure 1. (A) Relative changes in the color of a neutral aqueous solution containing a 20 mM 1:2 Co(II)/L-histidine mixture under N_2 (Deoxy-M) and O_2 (Oxy-M) atmosphere. The corresponding RGB-corrected spots are also demonstrated in the bottom panel for the solutions. Here, the RGB correction is performed by subtracting the RGB readings of the initial Deoxy-M sample. (B) Five consecutive cycles demonstrating the reversibility of the reaction. (C) Relative alteration of Deoxy-M and Oxy-M absorbances recorded at 410 nm with different O_2/N_2 cycling.

considered impractical due to their fragility *in vitro* and the cost associated with purifying an appreciable amount of proteins. Literature suggests a wide variety of naturally occurring and artificial cobalt complexes that bind with dioxygen.[16−19] Collman and group performed some early studies regarding the oxygen-binding potential of the "picket fence" system based on the substituted cobalt (II) phthalocyanine complex.[17] Here, the thermodynamic potential for oxygen bonding by a series of complexes was probed in both solid and liquid states. The same group also explored cobalt and iron-containing aza-capped porphyrins that structurally mimicked the heme protein active sites. This investigation provided fundamental insight into the structure-induced stabilization of oxygen adduct and destabilization of CO derivatives.[16] Martell and co-workers studied the oxygen affinity properties of various substituted Co(II) salen-type scaffolds to notice the effect of substituents on oxygen-binding ability as electron-withdrawing properties lower the oxygen-binding affinity.[18] There was an attempt to imitate the unique color-specific reversible O_2 binding of the natural metalloproteins with a cobalt−histidine molecular complex $[Co(His)_2]$; however, its detailed structure-function relationship has not been established yet.[20,21]

Here, in this study, we have revived the importance of this $[Co(His)_2]$ complex and deployed it for rapid and straightforward detection of O_2 in an aqueous solution in a broad range (0.1−100%). The O_2-sensing ability of the cobalt complex was probed qualitatively and quantitatively via two distinctive approaches. In the direct approach, the color difference between the deoxy and oxy form was availed to establish the extent of oxygenation. The detailed structural analysis with the help of a set of complementary spectroscopic experiments established the formation of a *trans*-μ-1,2-Co(III)-peroxo moiety in the oxy form. This peroxo motif was released in the form of H_2O_2 with acidification, which established the foundation of the second indirect method of colorimetric O_2 detection with the rational inclusion of a follow-up I_2/starch/$Na_2S_2O_3$-based titration step. Both the colorimetric O_2 detection techniques provided improved resolution with the appropriate RGB correction software following the capture of the pictures with commonly available smartphones. These

https://doi.org/10.1021/acsomega.2c03904
ACS Omega 2022, 7, 27734−27741

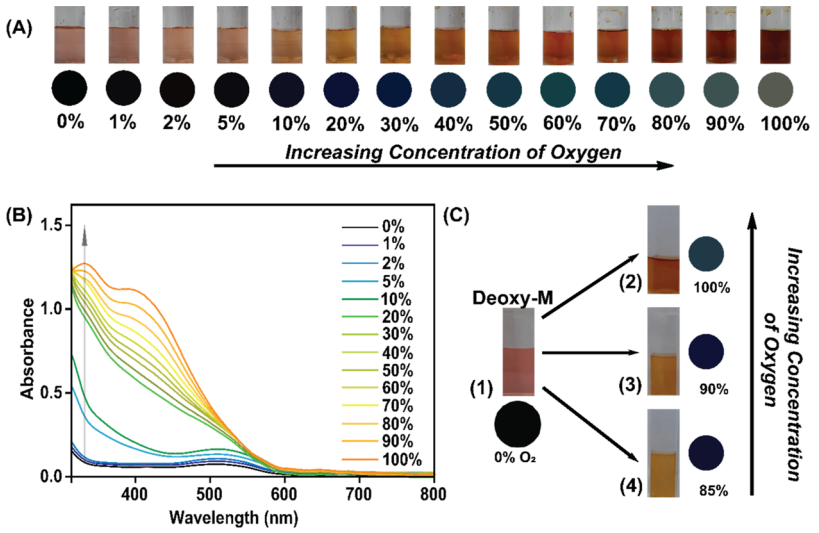

Figure 2. (A) Visible color pattern/colorimetric response (top) of the prepared oxygen sensor M under different concentrations of oxygen and RGB-corrected colors in circle (bottom). (B) Absorption spectra of M, in equilibrium with different oxygen concentrations in the surrounding atmosphere. (C) Real and RGB-corrected colors of (1) Deoxy-M, (2) Oxy-M (under 100% O_2), (3) Oxy-M (under 90% O_2), and (4) Oxy-M (under 85% O_2) observed during O_2 detection via the direct colorimetric method experiment.

processes displayed excellent colorimetric O_2 sensing in a large range from a very minute concentration of 0.1% to as high as 100% O_2 saturation level with excellent reproducibility. Hence, this study sets up a unique template for designing molecular complexes for oxygen-sensing applications, with rational incorporation of earth-abundant transition metals into natural amino acid-based ligand frameworks.

EXPERIMENTAL SECTION

Materials and Methods. Methanol (AR grade) and diethyl ether (AR grade) were purchased from Finar Chemicals Ltd. India. $CoCl_2{\cdot}2H_2O$ was purchased from Sigma-Aldrich, and L-Histidine was purchased from Loba Chemie. The optical spectra were recorded using an Ocean Insight USB2000+XR1-ES spectrophotometer, with the DT-MINI-2-GS light source using 1 cm path length in a 1 mL Kozima-made quartz cuvette. The ATR-FTIR spectra of pure solid samples were recorded on a PerkinElmer spectrometer. The atmosphere with different oxygen concentrations was created by a calibrated Mettler Toledo M800 Transmitter with an InPro 6000 Optical Sensor. The pH values of the aqueous solution were measured in a benchtop ORION STAR A111 pH Meter (Thermo Scientific).

Preparation of Deoxy-M and Oxy-M. The synthesis of the Deoxy-M and Oxy-M forms of the modeled $Co(His)_2$ complex (M) was done as per the reported procedure (Scheme 1). Initially, two separate aqueous solutions of $CoCl_2{\cdot}6H_2O$ (0.02M) and L-histidine (0.04M) were prepared at room temperature and were completely deoxygenated/deaerated by constant purging of argon for a few minutes. The solution of L-histidine was then added dropwise into the $CoCl_2{\cdot}6H_2O$ solution under inert conditions to obtain a pink color solution of the Deoxy-M complex. Addition of dioxygen gas to this aqueous solution of Deoxy-M results in a rapid color change to reddish brown corresponding to the Oxy-M complex (Figure 1).

RESULTS AND DISCUSSION

A minimalistic synthetic model of O_2-carrying metalloenzymes was developed by coordinating two equivalents of L-histidine to a Co(II) center in a neutral aqueous solution.[15,20−26] The initial metalation was performed under argon (Ar) atmosphere to originate a pink-colored deoxygenated version of the complex (Deoxy-M). This Deoxy-M complex spontaneously turned brown following its exposure to O_2, and it was assigned as the oxygenated metal complex (Oxy-M) (Figure 1A). The absolute shade of the solution was directly dependent on the extent of stoichiometric oxygenation of Deoxy-M, i.e., the concentration of oxygen present in the solution. Hence, the Deoxy-M complex has the potential to act as a chemical sensor for detecting molecular oxygen in the aqueous phase. The color difference between Deoxy-M and Oxy-M was digitalized with RGB values for its practical application (Figure 1A). The distinct color change between Deoxy-M and Oxy-M is reversible in nature, and their color reversal was further corroborated with the change in optical spectra and was repeated for five consecutive cycles with the sequential exposure of the solution to O_2 and Ar (Figure 1B,C).

This O_2-dependent color change of the Co(L-His)$_2$ complex was probed further as an analytical tool for detecting the variations of O_2 concentration ranging from minute 1% to complete saturation (100%), with a special emphasis on the medically relevant 80−100% purity zone. We have investigated the bioinspired Co(L-His)$_2$ complex-driven colorimetric O_2 assessment via two distinct pathways as described in the following sections.

Colorimetric Differentiation of O_2. *1A Direct Colorimetric O_2 Detection Method.* The presence of a minuscule amount of O_2 triggered the stoichiometric transformation of the Deoxy-M complex (pink) to Oxy-M (reddish-brown) in an aqueous solution under ambient conditions, which is generated through a stoichiometric reaction between molecular oxygen and Deoxy-M (*vide infra*). Henry's law describes that at a constant temperature, the dissolved O_2 in an aqueous solution is directly proportional to the partial pressure of the same gas present over the liquid−gas interface. Thus, the color change

https://doi.org/10.1021/acsomega.2c03904
ACS Omega 2022, 7, 27734−27741

occurring in the solution can reflect the slightest variation of different gas samples with contrasting O_2 concentrations.

A pure Deoxy-M sample in a neutral aqueous solution (pH 7.0) was prepared under strict anoxygenic conditions (100% Ar atmosphere) and designated as the 0% O_2 sample. Then, this sample was exposed to varying O_2 concentrations (0−100%), and the resultant change in the coloration of the stock solution was recorded (Figure 2A). A fluorescent oxygen gas sensor probe was employed to quantitatively adjust the O_2 concentration in these sample solutions. The inclusion of O_2 readily changes the color of the Deoxy-M sample, which is also apparent with the formation of signature bands around 350 nm and 410 nm in its absorption spectra (Figure 2B). The colorimetric change of the solution was observed even with the inclusion of very low concentrations of oxygen (Figure 2A and B). Hence, this process is potentially suitable for the detection of oxygen in adverse and hostile environmental conditions where absolute oxygen concentrations are critical. However, the difference in coloration of the Oxy-M sample was not evident to the naked eye between 80 and 100% O_2 saturation. To overcome this issue, the respective RGB values for each sample were fetched with a commonly available 64-megapixel primary camera (Sony IMX682 sensor used in this work) present in typical smartphones along with RGB-detecting software (*Color picker* or *RGB detector*), and they were subtracted from the RGB value recorded for the original Deoxy-M sample. The difference in the RGB-corrected features was distinctly observed for different O_2-saturated samples (Figure 2A). This colorimetric technique specifically depends on the dissolved O_2 concentration in a sample, which alters with varying temperatures. Next, we followed the efficiency of Deoxy-M to Oxy-M species formation in the 25−55 °C range to probe the temperature dependence of this O_2 detection methodology. The optical spectral data indicated that reliable Oxy-M generation ceases beyond 40 °C, whereas its maximum production was observed around room temperature (Figure S1).

We specifically probed the efficiency of this colorimetric method in the medically relevant zone (i.e., 85−100% O_2). For this purpose, we prepared a Deoxy-M solution under anoxygenic conditions and exposed it to the 85−100% O_2 concentration to record the corresponding colorimetric responses (Figure 2C). Although this methodology provides a rapid and reliable O_2 sensing handle over a broad range (0−100%), it failed to produce a clearly distinguishable change. These data display the potential of this bioinspired cobalt-amino acid complex for visual detection of oxygen concentration only in a broader range.

1B Indirect Colorimetric O_2 Detection Method. As mentioned in the previous section, one of the drawbacks of the direct colorimetric method was the minimal visual distinction observed for Co(L-His)$_2$ samples exposed to 85−90% O_2. Hence, we attempted to widen the scope of visible changes in these samples by rational utilization of an auxiliary chemical reaction. The spectroscopic experiments with Oxy-M samples demonstrated the formation of a peroxo functionality following the O_2 purging (*vide infra*). This peroxide intermediate can be extracted as hydrogen peroxide (H_2O_2) following the addition of an acid to the Oxy-M solution. The formation of H_2O_2 directly reflects the amount of O_2 present in the solution as they are stoichiometrically linked.

$$3I^-(aq) + H_2O_2(aq) + 2H^+(aq) \rightarrow I_3^-(aq) + 2H_2O(l) \quad (1)$$

$$2I_3^- + 1\%\ \text{starch (aq)} \rightarrow \text{starch}{-}I_5^-\ \text{complex (aq)} + I^-(aq) \quad (2)$$

$$I_3^-(aq) + 2S_2O_3^{2-}(aq) \rightarrow 3I^-(aq) + S_4O_6^{2-}(aq) \quad (3)$$

Now, the quantitative measurement of H_2O_2 via the back titration with $I^-/I_2/Na_2S_2O_3$ is a well-established analytical technique that can be employed here strategically for an indirect measurement of O_2 concentration in an aqueous solution. Here, the Oxy-M solution released H_2O_2 with the addition of 1M HCl solution. The Oxy-M complex was dismantled in this step, evident from a sharp change of solution color: reddish-brown to pink (Figure 3). The liberated H_2O_2 was subsequently deployed to oxidize an equivalent amount of iodide (added as excess KI) to I_2, which was illustrated by the brownish appearance of the solution (Figure 3). Next, a starch solution was added to this I_2-containing solution, which rapidly turned dark blue. The formation of starch−I_5^- adduct presumably originates from this solution that can be titrated with the reducing agent $Na_2S_2O_3$.[27] Now, this reaction between $Na_2S_2O_3$ and the starch-bound I_5^- sample is stoichiometric in nature, and the extent of this reaction can be fine-tuned with the addition of the specific amount of reducing agent $Na_2S_2O_3$ (eq 3). Next, we calculated the amount of $Na_2S_2O_3$ required to neutralize starch−I_5^- adduct generated from the exposure of 100% pure O_2 (via Oxy-M). Then, only 0.85 equiv of $Na_2S_2O_3$ of that maximal amount was added to the starch−I_5^- solution produced at the final step. Here, a pink solution was resulted for any sample exposed to ≤85% of O_2. On the other hand, a darker shade exists in the solution due to the presence of un-neutralized starch−I_5^-

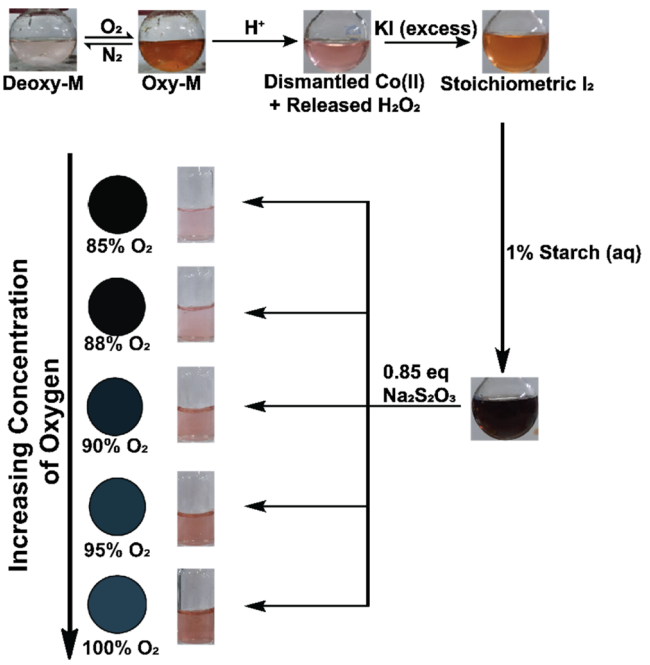

Figure 3. Serial changes in the coloration observed during the indirect O_2 measurement via the Co(His)$_2$ complex, involving the generation of stoichiometric amount of H_2O_2 and subsequent iodometric titration. The differentiation between samples exposed to 85−100% O_2 is highlighted with an appropriate RGB correction.

https://doi.org/10.1021/acsomega.2c03904
ACS Omega 2022, 7, 27734−27741

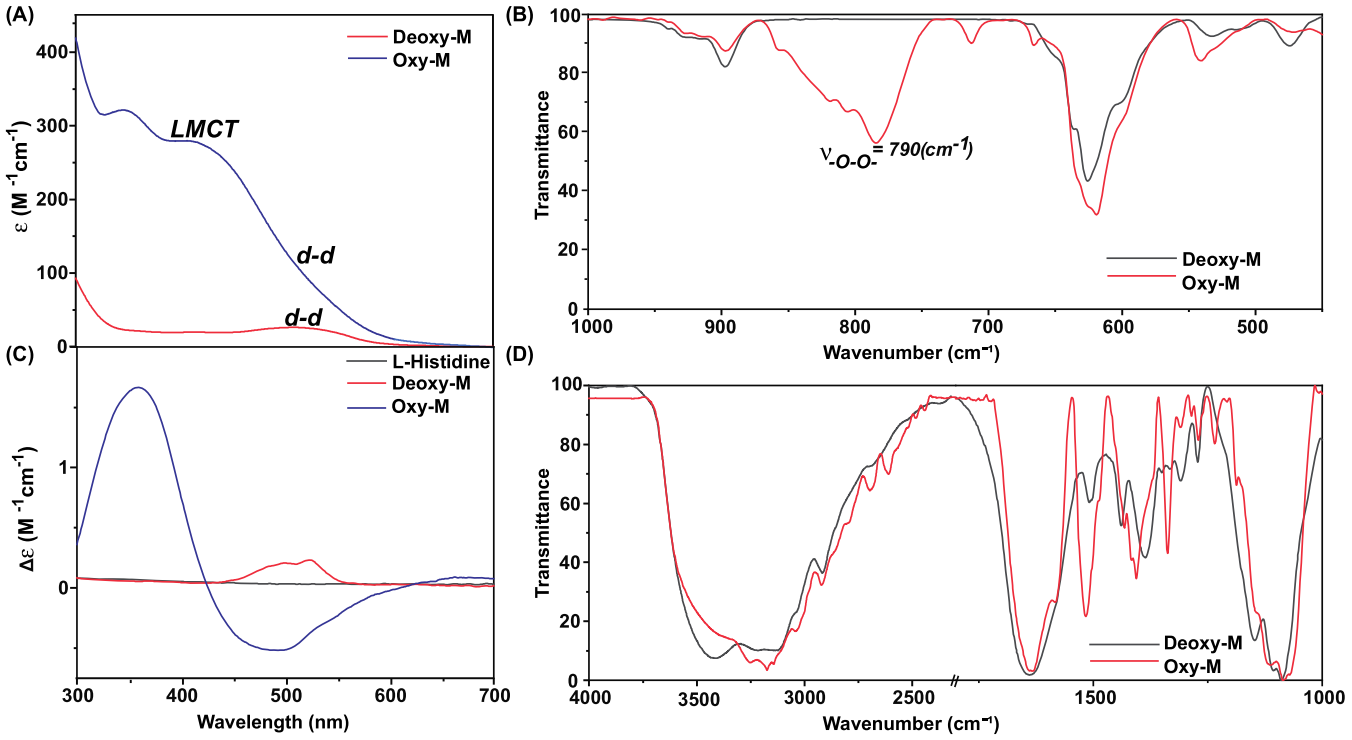

Figure 4. Comparative (A) optical and (C) corresponding CD spectra of the Deoxy-M (red trace) and Oxy-M (blue trace) complexes recorded in a neutral aqueous solution (pH 7.0), highlighting the respective LMCT and *d-d* transition bands and their changes following the oxygen exposure. The overlayed FTIR spectra for the Deoxy-M (red trace) and Oxy-M (blue trace) complexes measured in the (B) 450−1000 cm^{-1} and (D) 1000−400 cm^{-1} regions, highlighting the appearance of bridging peroxo stretching band and cobalt-bound L-histidine features, respectively. The FTIR data were recorded following the preparation of KBr pellets at room temperature.

adduct if the solution is purged with more than 85% O_2. This step was repeated with samples containing 85−100% of solvated O_2, where visibly distinct colors were observed. The resolution of the color difference for the samples exposed to 85−100% O_2 was intensified following the RGB correction (Figure 3).

The results display that the deoxy-M complex can act as a perfect chemical sensor for O_2 in an aqueous solution. Hence, this complex can be deployed further to establish a user-friendly and instrument-free analytical technique for O_2 purity check for rapid and distinctive colorimetric detection, akin to a pH indicator paper.

Deciphering the Mechanistic Details. The reaction between L-histidine and Co(II) possibly produces a 1:2 complex [Co(L-His)$_2$] (Deoxy-M) in a neutral aqueous solution under anaerobic conditions. The optical spectra of Deoxy-M present in a neutral aqueous solution exhibited a weak band around 510 nm (ε = 21 M^{-1} cm^{-1}) that was assigned as a *d-d* transition typically observed for octahedral Co(II) centers.[18] However, the spectral features altered significantly following the inclusion of molecular oxygen in the solution. Two new strong bands appeared at 350 nm (ε = 340 M^{-1} cm^{-1}) and 410 nm (ε = 300 M^{-1} cm^{-1}) in this Oxy-M sample; those were attributed to ligand-to-metal charge transfer (LMCT) transitions (Figure 4A). The appearance of two distinct LMCT bands possibly indicates the formation of a *trans-μ*-1,2-Co(III)-peroxo motif in the Oxy-M complex. The two LMCT bands are typically observed due to the high-energy $O_2^{2-}(\pi^*) \rightarrow$ Co(III)d_{z^2} (σ interaction) and relatively low-energy $O_2^{2-}(\pi^*) \rightarrow$ Co(III) $d_{x^2-y^2}$ (π interaction) transitions (Figure S2).[27] The possible formation of *trans-μ*-1,2-Co(III)-peroxo species was further supported by the complementary FTIR experiment performed with both the Deoxy-M and Oxy-M samples. The comparative FTIR spectra demonstrated the evolution of a sharp signal at 790 cm^{-1} exclusively for the Oxy-sample that can be accredited to the formation of metal-coordinated peroxo species analogous to a biological oxygen activator and carrier metalloproteins and their model complexes (Figure 4B).[10−26,28]

The strong electron delocalization between Co(III)-O_2^{2-}-Co(III) was further exemplified with the blue-shifted Co−L-His stretching signal ∼530 cm^{-1} (Figure 4B).[29,30] A change in the primary coordination sphere is warranted during the conversion of Deoxy-M to Oxy-M, which consists of a *trans-μ*-1,2-Co(III)-peroxo moiety. Here, one of the imidazole motifs possibly detaches from the cobalt, providing the ligation site for peroxo binding. The changes in the FTIR pattern ∼1100−1500 and 3000−3200 cm^{-1} regions corroborate the possible liberation of one of the imidazole groups, whereas the unaltered band at 1600 cm^{-1} signifies the intact Co-carboxylate bonds (Figure 4D).[31,32] The rearrangement of the metal coordination following the oxygen exposure was further probed with circular dichroism (CD) spectroscopy. The direct ligation of optically active L-His to cobalt induces chirality to the metal-based *d-d* optical transitions for the Deoxy-M sample. However, the spectral features altered considerably for the Oxy-M sample, where chiral LMCT bands appeared for this sample along with a stark change for *d-d* bands (Figure 4C). Such a gradual change in the CD spectral feature unequivocally supported the change of the coordination geometry around the cobalt center during the Deoxy-M-to-Oxy-M conversion (Figure S3). We propose the following molecular scheme that illustrates the possible sequential

https://doi.org/10.1021/acsomega.2c03904
ACS Omega 2022, 7, 27734−27741

Table 1. Spectral Data Comparison between the Deoxy-M and Oxy-M Samples

complex	optical spectral features [λ_{max}/nm (ε/M^{-1} cm^{-1})] (origin)	FTIR spectral features [$\bar{\nu}$/cm^{-1}] (origin)
Deoxy-M	510 (30) (*d-d*)	3120 ($\bar{\nu}^{as}_{NH_3^+}$, $\bar{\nu}^{as}_{NH_2}$, $\bar{\nu}_{imidazole}$); 1640 ($\bar{\nu}_{COO^-}$); 1510 ($\bar{\nu}_{C=N}$); 1386 ($\bar{\nu}_{C-N}$)
Oxy-M	350 (340), 410 (300) (LMCT); 550 (90), 700 (15) (*d-d*)	3250, 3180 ($\bar{\nu}^{as}_{NH_3^+}$, $\bar{\nu}^{as}_{NH_2}$, $\bar{\nu}_{imidazole}$); 1640 ($\bar{\nu}_{COO^-}$); 1515 ($\bar{\nu}_{C=N}$); 1405 ($\bar{\nu}_{C-N}$); 790 ($\bar{\nu}_{O-O}$)

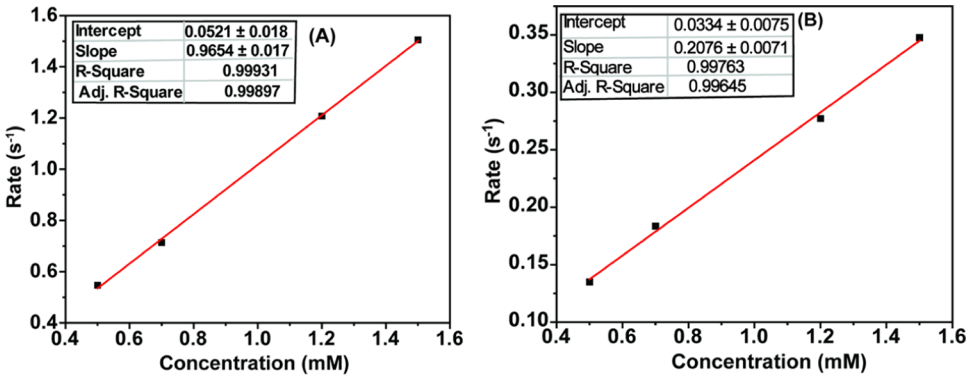

Figure 5. Rate of interconversion of the (A) Deoxy-M complex to the Oxy-M complex on addition of 100 μL of oxygen with varying metal concentrations. The rate of interconversion of the (B) Oxy-M complex to the Deoxy-M complex (with nitrogen purging) with varying metal concentrations with time.

changes in the Deoxy-M and Oxy-M samples after combining the insights from the optical, CD, and FTIR data (Scheme 1).

The preliminary generated pink Deoxy-M is mononuclear in nature, where the Co(II) center is coordinated with two molecules of tridentate L-histidine. This paramagnetic complex readily reacts with molecular oxygen and generates the brown-colored Oxy-M sample. Here, O_2 is reduced to peroxo (O_2^{2-} species) along with the Co(II)/Co(III) oxidation on two distinct Deoxy-M molecules. As a result, Oxy-M species is generated featuring a binuclear *trans*-μ-1,2-Co(III)-peroxo core. Here, a swift change in the coordination mode (tridentate to bidentate) of the L-histidine ligand plays a crucial role in harboring the peroxo ligand (Table 1).

Deciphering the Kinetics of Oxygen Sensing. The kinetics of interaction of the Co(II) complex with the molecular dioxygen was studied using optical spectroscopy where the change in absorbance at 410 nm was monitored with time following the addition of 100 μL of oxygen. The experiment was repeated for different complex concentrations keeping the oxygen concentration constant to obtain the oxygen-binding rate with varying metal concentrations. It was observed that the rate of oxygen binding enhanced with an increase in the metal concentration. A first-order rate constant of 0.965×10^{-3} s^{-1} was computed for the Deoxy-to-Oxy-M formation (Figure 5A). A continuous purging of nitrogen alters the course of the reaction and regenerates Deoxy-M from Oxy-M. This reaction was also examined via an analogous kinetic study, where a relatively slower rate constant (0.207×10^{-3} s^{-1}) was observed (Figure 5B).

CONCLUSIONS

The Co(L-histidine)$_2$ complex is reckoned as one of the bioinspired models of O_2-carrying metalloproteins that exhibit a swift change in color following exposure to O_2. We have demonstrated that the change of pink-colored Deoxy-M to the brown Oxy-M form can be employed for detecting the O_2 level present in an aqueous solution. This alteration establishes the platform for two distinct quantitative and qualitative colorimetric O_2 detection techniques. The first one is a direct method, where the color change in the solution was observed with a readily available smartphone camera and RGB detecting software. This user-friendly method reliably sensed O_2 from the minuscule level (0.1%) to the medically relevant (85−100%) zone. We have also established an indirect O_2 detection method as the Co(L-histidine)$_2$ complex produces a peroxo-bridged intermediate following its interaction with oxygen. We unleashed this stoichiometrically generated H_2O_2 with an acid treatment and determined its concentration with conventional I_2/starch/$Na_2S_2O_3$ titration. Here, the use of a specific amount of $Na_2S_2O_3$ allowed us to distinctly differentiate from 85 to 100% O_2 saturation. Next, we probed the molecular change in the complex structure following the O_2 treatment in detail with a battery of spectroscopic methods, including optical, FTIR, and CD. These studies suggested that O_2 binding triggers a significant change in the inner coordination sphere around cobalt. One of the imidazole groups gets disconnected to accommodate the peroxo bond formation, leading to a binuclear *trans*-μ-1,2-Co(III)-peroxo core. The present results provide a new perspective on developing bioinspired catalysts that can be utilized for colorimetric oxygen detection in a broad spectrum range for its widespread use in various industrial and medical fields.

ASSOCIATED CONTENT

Supporting Information

The Supporting Information is available free of charge at https://pubs.acs.org/doi/10.1021/acsomega.2c03904.

The figures depicting temperature effect on oxygen sensing, possible orbital interactions between Co and peroxide ion, comparative CD spectra of Oxy and Deoxy-M under partial oxygen pressure, and linear fit of absorbance value changes at 410 nm with variable compound concentration (PDF)

https://doi.org/10.1021/acsomega.2c03904
ACS Omega 2022, 7, 27734−27741

AUTHOR INFORMATION

Corresponding Authors

Debabrata Maiti − *Chemistry Department, Indian Institute of Technology Bombay, Mumbai 400076, India; Interdisciplinary Program in Climate Studies, Indian Institute of Technology Bombay, Mumbai 400076, India;* orcid.org/0000-0001-8353-1306; Email: dmaiti@iitb.ac.in

Arnab Dutta − *Chemistry Department, Indian Institute of Technology Bombay, Mumbai 400076, India; Interdisciplinary Program in Climate Studies and National Center of Excellence in CCU, Indian Institute of Technology Bombay, Mumbai 400076, India;* orcid.org/0000-0002-9998-6329; Email: arnab.dutta@iitb.ac.in

Authors

Abhishek Saini − *Chemistry Department, Indian Institute of Technology Bombay, Mumbai 400076, India*

Surabhi Rai − *Chemistry Department, Indian Institute of Technology Bombay, Mumbai 400076, India; National Center of Excellence in CCU, Indian Institute of Technology Bombay, Mumbai 400076, India*

Complete contact information is available at: https://pubs.acs.org/10.1021/acsomega.2c03904

Author Contributions

A.S. and A.D. conceptualized the project; A.S., S.R., and A.D. performed the experiments; A.S., S.R., D.M., and A.D. analyzed the data; A.S. and A.D. wrote the manuscript; A.S., S.R., D.M., and A.D. revised and edited the manuscript; A.D. supervised the project.

Notes

The authors declare no competing financial interest.

ACKNOWLEDGMENTS

The authors would like to thank the experimental facility and financial support provided by the Indian Institute of Technology Bombay (IITB). AS thanks CSIR for the financial fellowship support (09/087/(1075)-2020-I-EMR). SR and AD thank the support from DST (DST/TMD/CCUS/CoE/2020/IITB (G)).

REFERENCES

(1) Bruick, R. K.; McKnight, S. L. Oxygen Sensing Gets a Second Wind. *Science* **2002**, *295*, 807−808.

(2) Kocincová, A. S.; Nagl, S.; Arain, S.; Krause, C.; Borisov, S. M.; Arnold, M.; Wolfbeis, O. S. Multiplex Bacterial Growth Monitoring in 24-Well Microplates Using a Dual Optical Sensor for Dissolved Oxygen and PH. *Biotechnol. Bioeng.* **2008**, *100*, 430−438.

(3) Mills, A.; Lawrie, K.; Bardin, J.; Apedaile, A.; A Skinner, G.; O'Rourke, C. An O 2 Smart Plastic Film for Packaging. *Analyst* **2012**, *137*, 106−112.

(4) Roberts, L.; Lines, R.; Reddy, S.; Hay, J. Investigation of Polyviologens as Oxygen Indicators in Food Packaging. *Sens. Actuators, B* **2011**, *152*, 63−67.

(5) Smolander, M.; Hurme, E.; Ahvenainen, R. Leak Indicators for Modified-Atmosphere Packages. *Trends Food Sci. Technol.* **1997**, *8*, 101−106.

(6) Papkovsky, D. B. New Oxygen Sensors and Their Application to Biosensing. *Sens. Actuators, B* **1995**, *29*, 213−218.

(7) Shenoy, N.; Luchtel, R.; Gulani, P. Considerations for Target Oxygen Saturation in COVID-19 Patients: Are We under-Shooting? *BMC Med.* **2020**, *18*, No. 260.

(8) (a) Wilhelm, S.; Wolfbeis, O. S. Irreversible Sensing of Oxygen Ingress. *Sens. Actuators, B* **2011**, *153*, 199−204. (b) Mills, A.; Hazafy, D. A Solvent -Based Intelligence Ink for Oxygen. *Analyst* **2008**, *133*, 213−218. (c) Wang, X.-d.; S Wolfbeis, O. Optical Methods for Sensing and Imaging Oxygen: Materials, Spectroscopies and Applications. *Chem. Soc. Rev.* **2014**, *43*, 3666−3761. (d) Imran, M.; Chen, M. S. Self-Sensitized and Reversible O2 Reactivity with Bisphenalenyls for Simple, Tunable, and Multicycle Colorimetric Oxygen-Sensing Films. *ACS Appl. Mater. Interfaces* **2022**, *14*, 1817−1825.

(9) Wang, X.-d.; Chen, X.; Xie, Z.; Wang, X. Reversible Optical Sensor Strip for Oxygen. *Angew. Chem.* **2008**, *120*, 7560−7563.

(10) Wang, X.-d.; Meier, R. J.; Link, M.; Wolfbeis, O. S. Photographing Oxygen Distribution. *Angew. Chem., Int. Ed.* **2010**, *49*, 4907−4909.

(11) Evans, R. C.; Douglas, P.; Williams, J. A. G.; Rochester, D. L. A Novel Luminescence-Based Colorimetric Oxygen Sensor with a "Traffic Light" Response. *J. Fluoresc.* **2006**, *16*, 201−206.

(12) Frieden, E.; Osaki, S.; Kobayashi, H. Copper Proteins and Oxygen: Correlations between Structure and Function of the Copper Oxidases. *J. Gen. Physiol.* **1965**, *49*, 213−252.

(13) *The IUPAC Compendium of Chemical Terminology: The Gold Book*, 4th ed.; Gold, V., Ed.; International Union of Pure and Applied Chemistry (IUPAC): Research Triangle Park, NC, 2019 DOI: 10.1351/goldbook.

(14) Zijlstra, W. G.; Buursma, A.; Meeuwsen-van der Roest, W. P. Absorption Spectra of Human Fetal and Adult Oxyhemoglobin, de-Oxyhemoglobin, Carboxyhemoglobin, and Methemoglobin. *Clin. Chem.* **1991**, *37*, 1633−1638.

(15) Earnshaw, A.; Larkworthy, L. F. Structure of the Oxygen-Carrying Cobalt (II) Histidine Complex. *Nature* **1961**, *192*, 1068−1069.

(16) Niederhoffer, E. C.; Timmons, J. H.; Martell, A. E. Thermodynamics of Oxygen Binding in Natural and Synthetic Dioxygen Complexes. *Chem. Rev.* **1984**, *84*, 137−203.

(17) Chen, D.; Martell, A. E. Dioxygen Affinities of Synthetic Cobalt Schiff Base Complexes. *Inorg. Chem.* **1987**, *26*, 1026−1030.

(18) Collman, J. P.; Yan, Y.-L.; Eberspacher, T.; Xie, X.; Solomon, E. I. Oxygen Binding of Water-Soluble Cobalt Porphyrins in Aqueous Solution. *Inorg. Chem.* **2005**, *44*, 9628−9630.

(19) Collman, J. P.; Brauman, J. I.; Doxsee, K. M.; Halbert, T. R.; Hayes, S. E.; Suslick, K. S. Oxygen Binding to Cobalt Porphyrins. *J. Am. Chem. Soc.* **1978**, *100*, 2761−2766.

(20) Watters, K. L.; Wilkins, R. G. Interaction of Oxygen with the Cobalt(II)-Histidine Complex in Strongly Basic Solution. *Inorg. Chem.* **1974**, *13*, 752−753.

(21) Lever, A. B. P.; Gray, H. B. Electronic Spectra of Metal-Dioxygen Complexes. *Acc. Chem. Res.* **1978**, *11*, 348−355.

(22) Pająk, M.; Woźniczka, M.; Vogt, A.; Kufelnicki, A. Reversible Uptake of Molecular Oxygen by Heteroligand Co(II)−l-α-Amino Acid−Imidazole Systems: Equilibrium Models at Full Mass Balance. *Chem. Cent. J.* **2017**, *11*, No. 90.

(23) Morris, P. J.; Martin, R. B. Tetrahedral Complexes of Cobalt(II) with L-Histidine, Histamine, Imidazole, and N-Acetyl-L-Histidine. *J. Am. Chem. Soc.* **1970**, *92*, 1543−1546.

(24) Rafiquee, M. Z. A.; Siddiqui, M. R.; Al-Lohedan, H. A.; Al-Othman, Z. A. Kinetic Investigation on the Oxidation of N-Acetyl Cysteine by Dioxygen of μ-Dioxytetrakis(Histidinato)Dicobalt(II) Complex. *J. Mol. Liq.* **2017**, *229*, 424−428.

(25) Morris, P. J.; Bruce Martin, R. Stereoselective Formation of Cobalt(II), Nickel(II) and Zinc(II) Chelates of Histidine. *J. Inorg. Nucl. Chem.* **1970**, *32*, 2891−2897.

(26) Simplicio, Jon.; Wilkins, R. G. Kinetics of the Rapid Interaction of Bis(Histidinato)-Cobalt(II) with Oxygen. *J. Am. Chem. Soc.* **1967**, *89*, 6092−6095.

(27) Madhu, S.; Evans, H. A.; Doan-Nguyen, V. V. T.; Labram, J. G.; Wu, G.; Chabinyc, M. L.; Seshadri, R.; Wudl, F. Infinite Polyiodide Chains in the Pyrroloperylene−Iodine Complex: Insights into the

Starch−Iodine and Perylene−Iodine Complexes. *Angew. Chem., Int. Ed.* **2016**, *55*, 8032−8035.
(28) Solomon, E. I.; Tuczek, F.; Root, D. E.; Brown, C. A. Spectroscopy of Binuclear Dioxygen Complexes. *Chem. Rev.* **1994**, *94*, 827−856.
(29) Köse, D. A.; Necefoğlu, H. Synthesis and Characterization of Bis(Nicotinamide) m-Hydroxybenzoate Complexes of Co(II), Ni(II), Cu(II) and Zn(II). *J. Therm. Anal. Calorim.* **2008**, *93*, 509−514.
(30) Dolui, D.; Khandelwal, S.; Shaik, A.; Gaat, D.; Thiruvenkatam, V.; Dutta, A. Enzyme-Inspired Synthetic Proton Relays Generate Fast and Acid-Stable Cobalt-Based H2 Production Electrocatalysts. *ACS Catal* **2019**, *9*, 10115−10125.
(31) Petrosyan, A. M. Vibrational Spectra of L-Histidine Perchlorate and l-Histidine Tetrafluoroborate. *Vib. Spectrosc.* **2007**, *43*, 284−289.
(32) Barth, A. The Infrared Absorption of Amino Acid Side Chains. *Prog. Biophys. Mol. Biol.* **2000**, *74*, 141−173.

https://doi.org/10.1021/acsomega.2c03904
ACS Omega 2022, 7, 27734−27741